Large rapidity gap events in deep inelastic scattering

M. Wüsthoff
High Energy Physics Division, Argonne National Laboratory, Argonne, Illinois 60439
(Received 13 February 1997)

Large rapidity gap events in deep inelastic scattering are discussed in terms of light cone wave functions for quarks and gluons inside the photon. It is shown that this approach is consistent with earlier, conventional Feynman diagram calculations. An updated parametrization for the cross section is given and a numerical analysis presented. [S0556-2821(97)03119-6]

PACS number(s): 13.60.Hb, 12.38.Bx, 12.40.Nn

I. INTRODUCTION

With the start of DESY HERA a new tool has become available which allows a significant progress in sorting out the longstanding puzzle about the nature of the Pomeron [1,2]. Theoretically the Pomeron is difficult to tackle. It was introduced phenomenologically as a simple moving pole in the complex angular momentum plane (Pomeron trajectory) analogous to meson exchanges; however, compared to mesons there is no clear evidence for associated bound states in the s channel (candidates are glueballs). The Pomeron intercept is slightly above one which translates into a slowly growing total and elastic cross section in hadron reactions [3] (soft Pomeron). Meson trajectories, on the other hand, are below one and give subleading contributions at very high energies. Within the framework of perturbative QCD the Pomeron is associated with the resummation of leading logarithms in s (total energy) which results in a more complicated branch point singularity instead of a simple pole [4] (hard Pomeron). The major shortcoming of this leading $\ln(s)$ approach is the ignorance of nonperturbative contributions and the neglect of unitarity corrections which are relevant for the complete formation of the Pomeron [5,6]. Other approaches propose a combination of soft and hard Pomeron (see, for example, [7,8]) where the Pomeron intercept is controlled by the relevant scale of the process.

Due to its zero color charge the Pomeron is associated with the occurrence of rapidity gaps at very high energies. The simplest form of rapidity gap events beside elastic scattering is single diffraction where only one of the incoming particles dissociates (the virtual photon in deep inelastic scattering) whereas the other (the proton) stays intact. In most cases the proton escapes undetected, but it is surrounded by a large rapidity gap, a fact which is used in experiment to define diffraction. In the following we will assume the proton not to decay.

Deep inelastic scattering exhibits the nice feature of having a small colorless particle, the virtual photon, in the initial state. We will make use of this fact and shift the focus from the less well defined Pomeron to the virtual photon which we believe is perturbatively calculable, i.e., its content of quarks and gluons can be determined. Going into the target rest frame the following picture emerges: a fast traveling photon dissociates far upstream the proton-target into a quark-antiquark pair which evolves into a more complex partonic system before the actual interaction takes place. The initial separation of the quark-antiquark pair in impact parameter space is of the order of $1/Q$ (Q^2 is the photon virtuality). The final partonic system, however, which takes part in the interaction covers a much larger area roughly the size of a hadron. It appears to be rather natural to refer to the leading order quark-antiquark pair as a color dipole, it is less trivial, though, for a multiparticle state. Still, it may be shown that for leading twist contributions the concept of a color dipole can be extended to a more complicated final state. The argument goes as follows: hard QCD radiation generates a bunch of partons strongly ordered in impact parameter space. The large distance is marked by the last quark or gluon in the chain of emissions, whereas the remaining partons are confined in a small area (short distances). The separated parton, on the one hand, and the confined system of partons on the other hand form a new effective dipole. Both types, the quark dipole and the gluon dipole, can be described in terms of light cone wave functions. The gluon dipole, although it is of higher order in perturbation theory, is of particular relevance when the invariant mass M of the diffractive final state becomes large. The dipole picture is certainly limited in its applicability, but it works fine when Q^2 is the leading scale in the process, i.e., M^2/Q^2 is not extremely large.

For the interaction of the color dipole with the proton we employ the two gluon model [9]. All possible couplings have to be added up in order to retain gauge invariance. The two gluon model itself may not account for the full structure of the Pomeron, but it can be generalized to the exchange any number of gluons, since all gluons hooked on to one leg of the dipole can be merged into a single effective vertex. The strategy in this paper is to factorize the Pomeron structure from the dipole according to the k_t-factorization theorem [10]. The dipole part is calculated whereas the Pomeron part acquires a phenomenological parametrization. A full QCD treatment is not feasible at the present time. All free parameters will be determined from inclusive deep inelastic scattering data (F_2) and then used for diffraction.

In the following section we will introduce the light cone wave function formalism which includes an improved expression for the gluon dipole. In Sec. III the model for the Pomeron is specified and a fit to F_2 data which determines all parameters is performed. The Pomeron model is then combined with the light cone wave functions and the cross section for diffraction in deep inelastic scattering is calculated. It is shown that these results are consistent with earlier approaches based on more conventional calculations using

Feynman diagrams (Sec. IV). In Sec. V the cross section is numerically evaluated and the main results are discussed.

II. LIGHT CONE WAVE FUNCTIONS

One should take the terminology ''wave function'' not too literally, since the state it is meant to represent is not real but virtual. Still, it provides an effective and intuitive description of quark dipoles and gluon dipoles inside the photon in close analogy to a quark-antiquark bound state (quarkonium). An unpleasant property which can be traced back to the pointlike nature of the photon is the lack of normalizability of the wave function unlike for real states. In order to find the correct normalization one has to go back to the corresponding Feynman diagrams [11,12]. The nice feature is that once having determined the light cone wave function one can easily study single gluon and multigluon exchange, although the wave function formalism for the gluon dipole is restricted to color zero exchange, i.e., it works for two or multigluon exchange.

The virtual photon can be transverse polarized (transverse with respect to the light cone vectors $q'=q+x_Bp$ and p, q is the photon momentum and p the momentum of the incoming proton) as well as longitudinally polarized. The two helicity states $\gamma=\pm1$ follow from the projection on the transverse vectors $(1,i)$ and $(1,-i)$. For the left- and right-handed quarks we introduce the quark helicity $h=\pm1$. The quark momentum k may be parametrized as $k=\alpha q'+\beta_k p+k_t$ (Sudakov parametrization) which simultaneously fixes the decomposition of the antiquark momentum: $q-k=(1-\alpha)q'+(-x_B-\beta)p-k_t$. Using complex notation for the two-dimensional vector k_t we may write the light cone wave function for the quark-antiquark state as:

$$\Psi_h^\gamma(\alpha,k_t)=\begin{cases}\dfrac{\sqrt{2}(\alpha-1)k_t}{|k_t|^2+\alpha(1-\alpha)Q^2} & \text{for } \gamma=+1 \text{ and } h=+1,\\[2ex] \dfrac{\sqrt{2}\alpha k_t}{|k_t|^2+\alpha(1-\alpha)Q^2} & \text{for } \gamma=+1 \text{ and } h=-1,\\[2ex] \dfrac{\sqrt{2}\alpha k_t^*}{|k_t|^2+\alpha(1-\alpha)Q^2} & \text{for } \gamma=-1 \text{ and } h=+1,\\[2ex] \dfrac{\sqrt{2}(\alpha-1)k_t^*}{|k_t|^2+\alpha(1-\alpha)Q^2} & \text{for } \gamma=-1 \text{ and } h=-1\end{cases} \tag{1}$$

and

$$\Psi_h^\gamma(\alpha,k_t)=2\frac{\alpha(1-\alpha)Q}{|k_t|^2+\alpha(1-\alpha)Q^2} \quad \text{for } \gamma=0 \text{ and } h=\pm1, \tag{2}$$

where $Q^2=-q^2$ is the virtuality of the photon. Equation (2) shows the light cone wave function of the longitudinally polarized photon.

Before discussing the properties of the light cone wave function it is necessary to have a closer look at the kinematics. We assume that either the quark is off-shell and the antiquark on-shell or vice versa [here, $(q-k)^2=0$ and $k^2\neq0$, Fig. 1]. In the frame that we choose the photon moves fast and the two quarks roughly carry the momenta $\alpha q'$ and $(1-\alpha)q'$, whereas the other components are small. Any subsequent high-energy scattering does not change the α component. The off-shell quark with the momentum k becomes onshell after receiving a small fraction $x_{\mathbb{P}}$ of momentum along p while being scattered. The momentum of the quark changes from k to $\tilde{k}$ with $\tilde{k}^2=0$. Using the mass-shell condition one finds

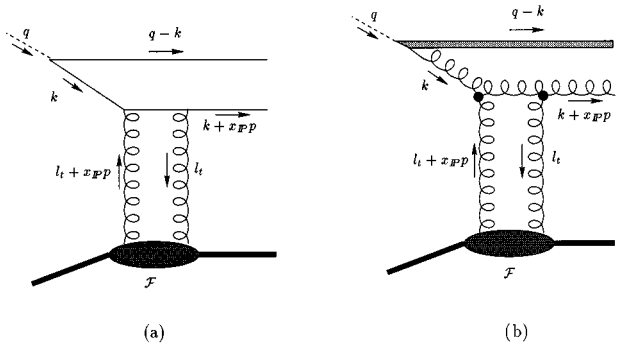

FIG. 1. Quark dipole (a) and gluon dipole (b).

$$\tilde{k}=\alpha q'+\frac{|k_t|^2}{\alpha W^2}p+k_t,$$

$$q-k=(1-\alpha)q'+\frac{|k_t|^2}{(1-\alpha)W^2}p-k_t. \tag{3}$$

W is the total hadronic mass ($W^2=2q'\cdot p$). The missing mass M is simply given as the total energy of the two outgoing quarks:

$$M^2=(\tilde{k}+q-k)^2=\left(q'+\frac{|k_t|^2}{\alpha(1-\alpha)W^2}p\right)^2=\frac{|k_t|^2}{\alpha(1-\alpha)}. \tag{4}$$

We now include the emission of a gluon in our discussion. At large M the gluon is well separated in rapidity from the $q\bar{q}$ pair and becomes the dominant configuration over the exclusive $q\bar{q}$-pair production. The latter is suppressed by a power in M^2 (spin-1/2 exchange). Unfortunately, the three particle Fock state is much more complicated, and a rigorous construction of the wave function which is consistent with Feynman rules and valid for all kinematics has not been achieved, yet. A simplification occurs when only the leading twist and leading $\ln(Q^2)$ contribution is considered. In this case the distance in the impact parameter space between the quark and the antiquark is much smaller than the distance between the quarks and the gluon. The $q\bar{q}$ pair on the one side and the gluon on the other side form an effective color dipole similar to the exclusive $q\bar{q}$ pair that we have considered before [Fig. 1(b)].

For the gluon dipole we find the following wave function [after introducing the vector notation $k_t=(k_t^1,k_t^2)$]:

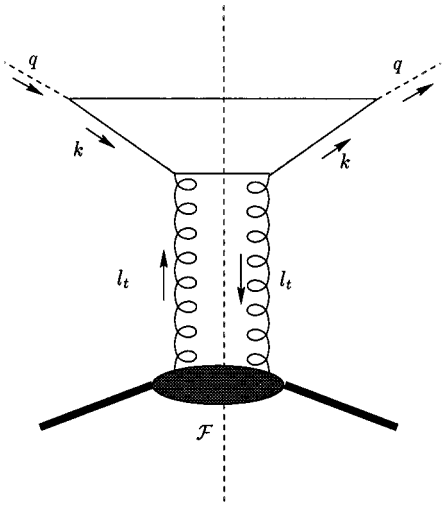

FIG. 2. Inclusive deep inelastic scattering (F_2).

$$\Psi^{mn}(\alpha,k_t)=\frac{1}{\sqrt{\alpha(1-\alpha)Q^2}}\,\frac{k_t^2\delta^{mn}-2k_t^m k_t^n}{k_t^2+\alpha(1-\alpha)Q^2}. \qquad (5)$$

In view of the two-vector-particles state (an effective two gluon state) it appears rather natural to find a tensor representation for the wave function. In the triple Regge limit (TRL) with M^2 much larger than Q^2 the term $\alpha(1-\alpha)Q^2$ in the denominator of Eq. (5) may be neglected and only k_t^2 remains:

$$\Psi^{mn}_{\mathrm{TRL}}(\alpha,k_t)=\frac{1}{\sqrt{\alpha(1-\alpha)Q^2}}\,\frac{2k_t^m k_t^n}{k_t^2}. \qquad (6)$$

The δ term which at first sight should be kept was also removed, since it does not depend on k_t and drops out in any application due to subtractions [see Eq. (19) of Sec. IV]. The simple structure of Eq. (6) was found earlier in Refs. [11,13]. Expression (5), on the other hand, is valid for all masses and provides the natural extension of the triple Regge result.

We have to point out that the wave function introduced in Eq. (5) does not reproduce the amplitude for the single gluon t-channel exchange. Especially those contributions which are singular in the limit $M\to 0$ are absent. The reason for that lies in the fact that in the color singlet configuration all singular, soft terms cancel out. This cancellation can be illustrated by considering final state radiation off the $q\bar{q}$ pair. The soft terms add up when the $q\bar{q}$ pair is colored, they cancel each other, however, when the state is colorless.

We have written Eq. (5) in a symmetric way with respect to α and $1-\alpha$ in order to stress the similarity with the $q\bar{q}$ dipole. The gluon dipole considered here is actually very asymmetric which is a consequence of the leading twist approximation where the internal virtualities are much smaller than Q^2. From Eq. (3) we conclude that α has to be much smaller than 1 in order to fulfill the condition $k^2 \ll Q^2$. So, one could have set $1-\alpha$ in Eq. (5) equal to 1 without reducing the accuracy of the formula.

At very large masses M or small β the dipole picture becomes insufficient. Instead of logarithms in Q^2 we have to sum up logs in $1/\beta$ or M^2/Q^2. This leads to a new four-gluon

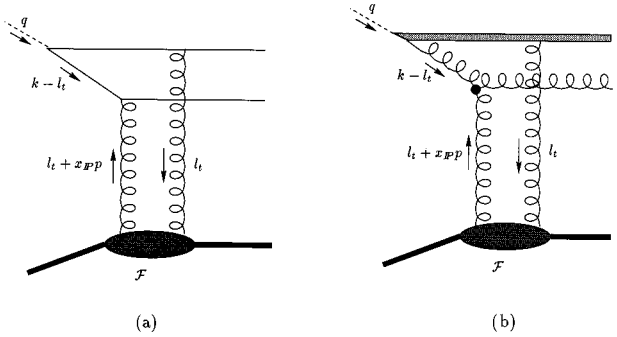

FIG. 3. Wave functions with shifted argument.

t-channel state [5,14] and a new singularity $1+\omega_4$ in the complex angular momentum plane [$(1/\beta)^{\omega_4}$]. But in contrast to conventional QCD-scaling violation the strong rise with $1/\beta$ does not imply a rise with Q^2.

III. MODELING THE STRUCTURE FUNCTION F_2

We compute the structure function F_2 at very low x_B when single gluon exchange gives the leading contribution. In contrast to the usual approach (gluon-boson fusion) the gluon is not on-shell and needs to be described by a distribution over both longitudinal and transverse phase space components (k_t factorization). Such a factorized distribution ($\mathcal{F}$) contains perturbative as well as nonperturbative contributions, and the aim is to find a suitable parametrization which gives a reasonable description of all low x_B and low Q^2 data.

The k_t-factorization theorem is the high energy or small x_B counterpart of the conventional (collinear) factorization theorem. The latter, when calculating the structure function F_2, requires a convolution of the gluon structure function and the quark box with respect to the longitudinal momentum fraction whereas in the small x_B regime the convolution with respect to the transverse momentum (k_t) is more appropriate. At zero momentum transfer the Pomeron (in deep inelastic scattering) is essentially the same as the unintegrated gluon structure function, and by fitting the F_2 data one determines the Pomeron intercept α_{P}. In deep inelastic scattering, however, the Pomeron intercept varies (depending on Q^2) rather than being a fixed number as in soft processes ($\alpha_{\mathrm{P}}=1.085$).

As we already mentioned one of the virtues of the wave function formalism is that we can use it for single gluon exchange (transverse momentum l_t) as well (see, Fig. 2). We find for F_2 the expression

$$F_2(x_B,Q^2)=\sum_f Q_f^2\,\frac{Q^2}{4\pi}\int\frac{d^2l_t}{\pi l_t^2}\mathcal{F}(x_B,l_t^2,Q_0^2)\times\int_0^1 d\alpha\int\frac{d^2k_t}{4\pi}\sum_{\gamma=0,+,-}\sum_{h=+,-}|\Psi_h^\gamma(\alpha,k_t)-\Psi_h^\gamma(\alpha,k_t+l_t)|^2. \qquad (7)$$

In the limit of large Q^2 (at fixed but small x_B) and taking

only the leading $\ln(Q^2)$ contribution the gluon distribution factorizes and the l_t integral can be taken:

$$x_B g(x_B,Q^2)=\int_0^{Q^2} dl_t^2 \frac{1}{\alpha_s}\mathcal{F}(x_B,l_t^2,Q_0^2). \tag{8}$$

$g(x_B,Q^2)$ represents the conventional gluon distribution and $\mathcal{F}/\alpha_s$ is usually referred to as unintegrated gluon structure function. Introducing the Feynman parameter x Eq. (7) reduces to

$$F_2(x_B,Q^2)=\sum_f Q_f^2\frac{Q^2}{4\pi}\int dl_t^2\mathcal{F}(x_B,l_t^2,Q_0^2)\int_0^1 dx\int_0^1 d\alpha\frac{[1-2x(1-x)][1-2\alpha(1-\alpha)]+8x(1-x)\alpha(1-\alpha)}{x(1-x)l_t^2+\alpha(1-\alpha)Q^2}. \tag{9}$$

This representation (see also, [16,17]) serves as starting point for further numerical evaluation.

As an ansatz for $\mathcal{F}$ we choose

$$\mathcal{F}(x_B,l_t^2,Q_0^2)=\frac{G(x_B,Q^2/Q_0^2)}{l_t^2+Q_0^2},$$

$$G(x_B,Q^2/Q_0^2)=A\left(\frac{x_B}{x_0}\right)^{1-\alpha_{\mathbb{P}}(Q^2)}\left[\ln\left(\frac{Q^2}{Q_0^2}\right)+1\right]^{-C}. \tag{10}$$

Q_0 is set to 1 GeV (proton mass), and since only small x_B are considered we introduced $x_0=0.05$ as normalization point. The Pomeron intercept has the parametrization

$$\alpha_{\mathbb{P}}(Q^2)=1.085+\begin{cases} B\ln[\ln(Q^2/Q_0^2)+1] & \text{if} \quad Q^2>Q_0^2, \\ 0 & \text{if} \quad Q^2\leqslant Q_0^2. \end{cases} \tag{11}$$

A soft Pomeron ($\alpha_{\mathbb{P}}=1.085$) intercept is assumed when the scale Q^2 falls below Q_0^2. This behavior has experimental support form the BPC data [18].

The ansatz in Eq. (10) has the following two basic ingredients: first, $\mathcal{F}$ scales such as $1/Q_0^2$ for $l_t=0$, i.e., an effective cutoff at the scale of Q_0^2 is introduced which eliminates the singularity related to the gluon propagator $1/l_t^2$. The scale Q_0 roughly represents the inverse size of the hadron and because hadrons are colorless all gluons with a wave length larger than the size of the hadron decouple. One important consequence is the vanishing of the structure function when Q^2 approaches zero. The second ingredient is a scale (Q^2-) dependent Pomeron intercept. It takes care of the experimental fact that the small-x_B rise becomes weaker when the scale decreases and finally turns into the soft behavior below Q_0. The parameter B in Eq. (11) has to be determined from data. Two more parameters come along with B [see Eq. (10)], A fixes the absolute normalization and C corrects the strong scaling violation which results from the scale dependent parametrization of the Pomeron intercept.

The data for the fit are taken from HERA [18,19] below $Q^2=50$ GeV^2 and from E665 [20] including the smallest Q^2 values. The fit gives the following values for the three parameters A,B, and C:

$$A=0.877,$$
$$B=0.133, \tag{12}$$
$$C=0.596.$$

These parameters will be used in the following to predict the diffractive structure function F_2^D.

IV. DIFFRACTION

For the diffractive cross section we use the same conventions as for the inclusive cross section in deep inelastic scattering, i.e., we decompose it into a transverse and a longitudinal part according to the different polarizations of the virtual photon:

$$\left.\frac{d\sigma}{d\beta dQ^2 dx_{\mathbb{P}} dt}\right|_{t=0}=\frac{\alpha_{em}}{2x_{\mathbb{P}}Q^4}\{-[1+(1-y)^2]x_B W_t +4(1-y)x_B W_l\}, \tag{13}$$

where W_t and W_l are the transverse and longitudinal projection of the hadronic tensor $W^{\mu\nu}$:

$$W_t=g_t^{\mu\nu}W_{\mu\nu},$$
$$W_l=\frac{4Q^2}{s^2}p^\mu p^\nu W_{\mu\nu}, \tag{14}$$

with $s=2q'\cdot p$ and $q'=q+x_B p$. The transverse tensor $g_t^{\mu\nu}$ is defined as

$$g_t^{\mu\nu}=g^{\mu\nu}-\frac{q'^\mu p^\nu+p^\mu q'^\nu}{q'\cdot p}. \tag{15}$$

The momentum transfer is set to zero, a restriction, which is justified by the fact that the cross section peaks at $t=0$.

At leading order we have to consider the coupling of two t-channel gluons to a quark-antiquark pair. The four possible couplings are represented by four terms involving the wave function with shifted transverse momenta [see Fig. 3(a)]. These shifts correspond to the transverse momenta carried by the gluons (l_t and $-l_t$) when the total momentum transfer is zero:

$$\int \frac{d^2l_t}{\pi l_t^2}\mathcal{F}(x_{\mathrm{P}},l_t^2,Q_0^2)[2\Psi_h^{\gamma}(\alpha,k_t)-\Psi_h^{\gamma}(\alpha,k_t+l_t)-\Psi_h^{\gamma}(\alpha,k_t-l_t)]$$

$$=\int \frac{dl_t^2}{l_t^2}\mathcal{F}(x_{\mathrm{P}},l_t^2,Q_0^2) \tag{16}$$

$$\times\begin{cases}\left[\dfrac{k_t^2-\alpha(1-\alpha)Q^2}{k_t^2+\alpha(1-\alpha)Q^2}-\dfrac{k_t^2-l_t^2-\alpha(1-\alpha)Q^2}{\sqrt{[k_t^2+l_t^2+\alpha(1-\alpha)Q^2]^2-4k_t^2l_t^2}}\right]\begin{cases}\dfrac{\sqrt{2}(\alpha-1)k_t}{|k_t|^2} & \text{for } \gamma=+1 \text{ and } h=+1,\\ \dfrac{\sqrt{2}\alpha k_t}{|k_t|^2} & \text{for } \gamma=+1 \text{ and } h=-1,\\ \dfrac{\sqrt{2}\alpha k_t^*}{|k_t|^2} & \text{for } \gamma=-1 \text{ and } h=+1,\\ \dfrac{\sqrt{2}(\alpha-1)k_t^*}{|k_t|^2} & \text{for } \gamma=-1 \text{ and } h=-1,\end{cases}\\ \left[\dfrac{2\alpha(1-\alpha)Q}{|k_t|^2+\alpha(1-\alpha)Q^2}-\dfrac{2\alpha(1-\alpha)Q}{\sqrt{[k_t^2+l_t^2+\alpha(1-\alpha)Q^2]^2-4k_t^2l_t^2}}\right] \quad \text{for } \gamma=0 \text{ and } h=\pm 1.\end{cases}$$

The last expression results after integration over the azimuthal angle.

For the total contribution to W_t and W_l one has to take the square of the amplitude, i.e., basically the square of the previous expression with summation over the corresponding helicities:

$$x_B W_t^{q\bar{q}}=-\sum_f Q_f^2\frac{\pi}{24}\frac{Q^2}{\beta(1-\beta)}\int_0^1 d\alpha[\alpha^2+(1-\alpha)^2]\left\{\int\frac{dl_t^2}{l_t^2}\mathcal{F}(x_{\mathrm{P}},l_t^2,Q_0^2)\right.$$
$$\left.\times\left[1-2\beta+\frac{\beta l_t^2/Q^2-(1-2\beta)\alpha(1-\alpha)}{\sqrt{[\beta l_t^2/Q^2+\alpha(1-\alpha)]^2-4\alpha(1-\alpha)\beta(1-\beta)l_t^2/Q^2}}\right]\right\}^2 \tag{17}$$

and

$$x_B W_l^{q\bar{q}}=\sum_f Q_f^2\frac{\pi}{3}Q^2\int_0^1 d\alpha\alpha(1-\alpha)\left\{\int\frac{dl_t^2}{l_t^2}\mathcal{F}(x_{\mathrm{P}},l_t^2,Q_0^2)\left[1-\frac{\alpha(1-\alpha)}{\sqrt{[\beta l_t^2/Q^2+\alpha(1-\alpha)]^2-4\alpha(1-\alpha)\beta(1-\beta)l_t^2/Q^2}}\right]\right\}^2. \tag{18}$$

We have here substituted k_t^2 using Eq. (4) in combination with $\beta=Q^2/(M^2+Q^2)$. Similar expressions can be found in [5,11,12]. As in the previous section we have absorbed the strong coupling constant into $\mathcal{F}$. This way the remaining expressions become free of parameters.

By taking the limits $\beta\to 1$ and $\beta\to 0$ one can study the main properties of Eqs. (17) and (18). For $\beta\to 1$ Eq. (17) vanishes proportional to $(1-\beta)$, whereas Eq. (18) gives a finite contribution. Hence, at small masses the longitudinal contribution is larger than the transverse contribution. A similar observation is made for vector meson production in deep inelastic scattering. One, however, has to be aware that the longitudinal part is of higher twist, so that the ratio of the transverse part to longitudinal does not vanish as M^2/Q^2 at large Q^2, but is roughly of the order of M^2/Q_0^2 with a logarithmic enhancement (see also Ref. [21]). Taking the second limit, $\beta\to 0$, one observes that the transverse contribution is finite, i.e., in terms of the mass M, the cross section vanishes as $1/M^4$ as expected for a spin-1/2 exchange. The longitudinal part (18) has an asymptotic behavior proportional to β^2, i.e., is negligible at large masses.

For the configuration with a gluon in the final state we go back to Eq. (5). As in Eq. (16) we encounter four terms [see Fig. 3(b)]:

$$\int \frac{d^2l_t}{\pi l_t^2}\mathcal{F}(x_{\mathbb{P}},l_t^2,Q_0^2)[2\Psi^{mn}(\alpha,k_t)-\Psi^{mn}(\alpha,k_t+l_t)-\Psi^{mn}(\alpha,k_t-l_t)]$$
$$=\int \frac{dl_t^2}{l_t^2}\mathcal{F}(x_{\mathbb{P}},l_t^2,Q_0^2)\frac{1}{\sqrt{\alpha(1-\alpha)Q^2}}\times\left[1-\frac{2k_t^2}{k_t^2+\alpha(1-\alpha)Q^2}-\frac{l_t^2}{k_t^2}-\frac{\alpha(1-\alpha)Q^2}{k_t^2}+\frac{[l_t^2-k_t^2+\alpha(1-\alpha)Q^2]^2+2k_t^2\alpha(1-\alpha)Q^2}{k_t^2\sqrt{[l_t^2+k_t^2+\alpha(1-\alpha)Q^2]^2-4l_t^2k_t^2}}\right]\times\left\{\frac{2k_t^mk_t^n}{k_t^2}-\delta^{mn}\right\}. \tag{19}$$

To get the complete contribution for W_t one has to, first, take the square of the previous expression and, second, add the contribution for the perturbative splitting of a gluon into two quarks:

$$x_BW_t^g=-\sum_f Q_f^2\frac{\pi}{2}\int_0^{Q^2}dk^2\frac{\alpha_s}{8\pi}\ln\left(\frac{Q^2}{k^2}\right)\int_\beta^1\frac{dz}{z^2}\left[\left(1-\frac{\beta}{z}\right)^2+\left(\frac{\beta}{z}\right)^2\right]\frac{9}{4}\frac{1}{(1-z)^2}\left\{\int\frac{dl_t^2}{l_t^2}\mathcal{F}(x_P,l_t^2,Q_0^2)\left[z^2+(1-z)^2+\frac{l_t^2}{k^2}-\frac{[(1-2z)k^2-l_t^2]^2+2z(1-z)k^4}{k^2\sqrt{(k^2+l_t^2)^2-4(1-z)l_t^2k^2}}\right]\right\}^2. \tag{20}$$

Two new variables were introduced in this equation, the longitudinal momentum fraction z (relative to the Pomeron momentum) and the virtuality k^2 of the t-channel gluon which is connected to the quark box. k^2 is related to the transverse momentum by $k^2=k_t^2/(1-z)$. The previously used variable α was substituted by means of the equation $\alpha(1-\alpha)Q^2=zk^2$ where we assume that $\alpha\ll 1$ according to the leading $\ln(Q^2)$ approach adopted here. A factor of two arises in the integration from the opposite and symmetric limit $(1-\alpha)\ll 1$. A contribution to W_l is negligible in this case. We, again, take the two limits $\beta\to 0$ and $\beta\to 1$ in order to understand the basic behavior. For small β the region of small z dominates, so that the second line in Eq. (20) can be approximated by setting z to zero. Integrating over z then results in $1/\beta$, i.e., the cross section is divergent when β approaches zero. The small β or triple Regge limit has already been considered before in Refs. [6,11–13,15], and the results are found to be consistent with our calculations. One can also start with Ψ^{mn}_{TRL} [Eq. (6)] which directly yields the triple Regge limit of Eq. (20). Taking the opposite limit $\beta\to 1$ which was not covered by previous calculations one finds that Eq. (20) vanishes as $(1-\beta)^3$. This result emerges by taking the limit $z\to 1$ resulting in $(1-z)^2$ and integrating over z. A derivation of Eq. (20) based on Feynman diagrams is given in Ref. [22].

It is important to note that the function $\mathcal{F}$ is assumed to be universal and should be the same for all three Eqs. (17), (18), and (20). The only parameter that enters in Eq. (20) is the strong coupling constant α_s. It depends on the scale somewhere between Q_0 and Q.

One may introduce a simplification by taking the limit $l_t\to 0$ in the wave functions of Eqs. (16) and (19). This limit gives the leading contribution provided that $k_t^2/(1-\beta)$ is much larger than Q_0^2:

$$\int\frac{d^2l_t}{\pi l_t^2}\mathcal{F}(x_{\mathrm{P}},l_t^2,Q_0^2)[2\Psi_h^\gamma(\alpha,k_t)-\Psi_h^\gamma(\alpha,k_t+l_t)-\Psi_h^\gamma(\alpha,k_t-l_t)]$$
$$\simeq\left[-2\frac{\partial^2\Psi_h^\gamma(\alpha,k_t)}{\partial k_t\partial k_t^*}\right]\int^{|k_t|^2+\alpha(1-\alpha)Q^2}dl_t^2\mathcal{F}(x_{\mathrm{P}},l_t^2,Q_0^2)$$
$$=\alpha_sx_{\mathrm{P}}g[x_{\mathrm{P}},|k_t|^2+\alpha(1-\alpha)Q^2,Q_0^2]$$
$$\times\left\{\frac{4\alpha(1-\alpha)Q^2}{[|k_t|^2+\alpha(1-\alpha)Q^2]^3}\begin{cases}\sqrt{2}(\alpha-1)k_t & \text{for } \gamma=+1 \text{ and } h=+1,\\ \sqrt{2}\alpha k_t & \text{for } \gamma=+1 \text{ and } h=-1,\\ \sqrt{2}\alpha k_t^* & \text{for } \gamma=-1 \text{ and } h=+1,\\ \sqrt{2}(\alpha-1)k_t^* & \text{for } \gamma=-1 \text{ and } h=-1,\end{cases}\right.$$
$$\left.\frac{\alpha(1-\alpha)Q^2-|k_t|^2}{[|k_t|^2+\alpha(1-\alpha)Q^2]^3}\quad 2\alpha(1-\alpha)Q \text{ for } \gamma=0 \text{ and } h=\pm 1.\right\} \tag{21}$$

One may call this result leading $\ln(k^2/Q_0^2)$ approach for the remaining integration over l_t^2 [Eq. (8)] is logarithmic (one propagator $1/l_t^2$ is hidden in $\mathcal{F}$). It also indicates the limitation to large k^2.

We again convert the previous results into contributions to W_t and W_l. Substituting α by means of Eq. (4) and introducing the virtuality $k^2=k_t^2/(1-\beta)$ we find

$$x_B W_t^{q\bar{q}} = -\sum_f Q_f^2 \frac{\pi}{3} 4\beta^2(1-\beta) \times \int_{k_0^2}^{Q^2} \frac{dk^2}{k^4} \{\alpha_s x_{\mathbb{P}} g(x_{\mathbb{P}}, k^2, Q_0^2)\}^2 \tag{22}$$

and

$$x_B W_l^{q\bar{q}} = \sum_f Q_f^2 \frac{\pi}{3Q^2} \beta^2(1-2\beta)^2 \times \int_{k_0^2}^{Q^2} \frac{dk^2}{k^2} \{\alpha_s x_{\mathbb{P}} g(x_{\mathbb{P}}, k^2, Q_0^2)\}^2. \tag{23}$$

Equation (22) was derived earlier in Refs. [23–26] and Eq. (23) in Ref. [26]. The virtue of this approach is the fact that we do not need the unintegrated structure function, instead we can use the conventional structure function. The shortcomings, however, are first of all the need of a cutoff k_0^2 which can only be realized by requiring jets in the final state. Second, one recognizes that in Eq. (22) the small β region is strongly suppressed and not constant as anticipated earlier. In this regime next-to-leading $\ln(k^2/Q_0^2)$ corrections become important. Corrections of this type have been explicitly calculated in [27]. We face a similar situation for the longitudinal contribution Eq. (23) which is zero at $\beta=1/2$. Again next-to-leading log contributions become relevant here.

To complete the discussion on the leading $\ln(k^2/Q_0^2)$ approach we give the corresponding formula for gluon production

$$\begin{aligned}
&\int \frac{d^2 l_t}{\pi l_t^2} \mathcal{F}(x_{\mathbb{P}}, l_t^2, Q_0^2)[2\Psi^{mn}(\alpha, k_t) - \Psi^{mn}(\alpha, k_t + l_t) \\
&\quad - \Psi^{mn}(\alpha, k_t - l_t)] \\
&\simeq \left[-\delta^{ij} \frac{\partial^2 \Psi^{mn}(\alpha, k_t)}{\partial k_t^i \partial k_t^j} \right] \\
&\quad \times \int^{|k_t|^2 + \alpha(1-\alpha)Q^2} dl_t^2 \mathcal{F}(x_{\mathbb{P}}, l_t^2, Q_0^2) \\
&= \frac{2k_t^2}{\sqrt{\alpha(1-\alpha)Q^2}} \frac{3\alpha(1-\alpha)Q^2 + k_t^2}{[k_t^2 + \alpha(1-\alpha)Q^2]^3} \left\{ \delta^{mn} - \frac{2k_t^m k_t^n}{k_t^2} \right\} \\
&\quad \times \alpha_s x_{\mathbb{P}} g[x_{\mathbb{P}}, |k_t|^2 + \alpha(1-\alpha)Q^2, Q_0^2].
\end{aligned} \tag{24}$$

As before we take the square of the previous expression and rewrite the result in terms of W_t^g. The procedure is similar to the derivation of Eq. (20), where $\alpha(1-\alpha)Q^2$ is substituted by zk^2 and the splitting function for gluons into quarks is added:

$$x_B W_t^g = -\sum_f Q_f^2 \frac{\pi}{2} \int_{k_0^2}^{Q^2} \frac{dk^2}{k^4} \frac{\alpha_s}{8\pi} \ln\left(\frac{Q^2}{k^2}\right) \int_\beta^1 \frac{dz}{z^2} \left[\left(1 - \frac{\beta}{z}\right)^2 + \left(\frac{\beta}{z}\right)^2 \right] 9(1+2z)^2(1-z)^2 \{\alpha_s x_{\mathbb{P}} g(x_{\mathbb{P}}, k^2, Q_0^2)\}^2. \tag{25}$$

This result has been derived earlier in Refs. [22,24,25] by direct calculation of Feynman diagrams.

V. NUMERICAL RESULTS

With the formulas for diffraction at hand and $\mathcal{F}$ determined by the inclusive F_2 (see Sec. II) we can numerically evaluate F_2^D. To this end we note that F_2^D and F_l^D are related to W_t and W_l by

$$F_2^D = \frac{\beta}{x_{\mathbb{P}}} \left(-\frac{x_b W_t}{4\pi} + \frac{x_b W_l}{2\pi} \right),$$

$$F_l^D = \frac{\beta}{x_{\mathbb{P}}} \frac{W_l}{4\pi}, \tag{26}$$

which follows from

$$\frac{d\sigma^D}{d\beta dQ^2 dx_p} = \frac{2\pi\alpha_{em}^2}{\beta Q^4} \{[1+(1-y)^2] F_2^D(\beta, Q^2, x_{\mathbb{P}}) - 2x_b y^2 F_l^D(\beta, Q^2, x_{\mathbb{P}})\}. \tag{27}$$

The longitudinal structure function F_l is usually negligible due to the accompanying factor y^2 which is experimentally small in most cases (y is the energy loss of the electron). But the longitudinal contribution is not completely lost, since it still appears in F_2^D [see Eq. (26)].

We insert the form factor $1/(l_t^2+Q_0^2)$ which belongs to $\mathcal{F}$ into Eqs. (17), (18), and (20) and perform the integration over l_t^2 analytically. For convenience we introduce the variable v which is defined as $v=Q_0^2/[k_t^2+\alpha(1-\alpha)Q^2] = Q_0^2(1-\beta)/k_t^2$ for the quark dipole and $v=Q_0^2/k^2 = Q_0^2(1-z)/k_t^2$ for the gluon dipole. F_2^D is then presented in three separate contributions ($F_2^D=F_a+F_b+F_c$) according to Eqs. (17)(F_a), (18)(F_b), and (20)(F_c)

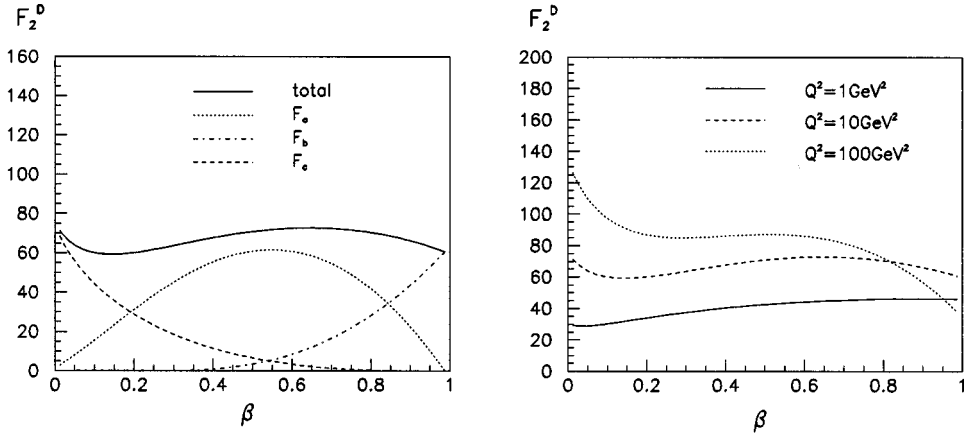

FIG. 4. β spectrum.

$$F_a(\beta,Q^2,x_p)=\frac{1}{12B_DQ_0^2}\int_{4\beta Q_0^2/Q^2}^{\infty}\frac{dv}{v^2\sqrt{1-4(Q_0^2\beta/Q^2v)}}G^2(x_p,1/v)\frac{\beta}{x_p}\left(1-2\frac{Q_0^2\beta}{Q^2v}\right)\frac{1}{6}\frac{1}{1-\beta}\left\{(1-2\beta)\ln\left(\frac{1}{\beta}\right)\right.$$
$$+\left(\frac{1-2\beta+v}{\sqrt{v^2+2(1-2\beta)v+1}}-1+2\beta\right)\ln(v)$$
$$\left.+\frac{1-2\beta+v}{\sqrt{v^2+2(1-2\beta)v+1}}\ln\left(\frac{\sqrt{v^2+2(1-2\beta)v+1}-(1-2\beta+v)}{\sqrt{v^2+2(1-2\beta)v+1}+(1-2\beta)v+1}\right)\right\}^2, \tag{28}$$

$$F_b(\beta,Q^2,x_p)=\frac{1}{6B_DQ^2}\int_{4\beta Q_0^2/Q^2}^{\infty}\frac{dv}{v^3\sqrt{1-4(Q_0^2\beta/Q^2v)}}G^2(x_p,1/v)\frac{\beta^3}{x_p}\frac{4}{3}\left\{\ln\left(\frac{1}{\beta}\right)+\left(\frac{1}{\sqrt{v^2+2(1-2\beta)v+1}}-1\right)\ln(v)\right.$$
$$\left.+\frac{1}{\sqrt{v^2+2(1-2\beta)v+1}}\ln\left(\frac{\sqrt{v^2+2(1-2\beta)v+1}-(1-2\beta+v)}{\sqrt{v^2+2(1-2\beta)v+1}+(1-2\beta)v+1}\right)\right\}^2, \tag{29}$$

and

$$F_c(\beta,Q^2,x_p)=\frac{1}{12B_DQ_0^2}\int_{Q_0^2/Q^2}^{\infty}\frac{dv}{v^2}G^2(x_p,1/v)\frac{\beta}{x_p}\frac{\alpha_s}{8\pi}\ln\left(\frac{vQ^2}{Q_0^2}\right)\int_\beta^1\frac{dz}{z^2}\left[\left(1-\frac{\beta}{z}\right)^2+\left(\frac{\beta}{z}\right)^2\right]\frac{9}{4}\frac{1}{(1-z)^2}$$
$$\times\left\{[1+v-2z(1-z)]\ln\left(\frac{1}{z}\right)+\ln(v)\left[v-1+2z(1-z)+\sqrt{v^2+2(1-2z)v+1}-\frac{2z(1-z)}{\sqrt{v^2+2(1-2z)v+1}}\right]\right.$$
$$\left.+\left[\sqrt{v^2+2(1-2z)v+1}-\frac{2z(1-z)}{\sqrt{v^2+2(1-2z)v+1}}\right]\ln\left(\frac{\sqrt{v^2+2(1-2z)v+1}-(1-2z+v)}{\sqrt{v^2+2(1-2z)v+1}+(1-2z)v+1}\right)\right\}^2. \tag{30}$$

Since the measurement is not performed at $t=0$ we have assumed a simple exponential behavior in t, $\exp(B_Dt)$, with the slope parameter B_D taken from experiment [28] ($B_D=5.9/\mathrm{GeV}^2$). The integration over t leads to the extra factor $1/B_D$. For α_s we estimate a value of 0.25 which is a reasonable estimation for scales around 2–3 GeV. The function G is defined in Eq. (10) and enters the equations above without changing the parameters. In Fig. 4 (first plot) we show the β distribution for fixed $x_{\mathbb{P}}=5.0\times10^{-4}$ and $Q^2=10$ GeV^2 with separate curves for each of the three contributions F_a,F_b, and F_c. As was already argued analytically we find three distinct regimes in the β spectrum: (i) small β where the configuration with a gluon in the final state dominates (F_c), (ii) medium β where the exclusive quark-antiquark production with transverse polarization is dominant (F_a), and (iii) large β where the longitudinal production of quark-antiquark pairs takes over (F_b). The second plot displays the change in the shape of the β distribution with increasing Q^2. It is rather flat around $Q^2=10$ GeV^2 before it starts tilting when Q^2 is further increased (higher twist suppression at the large end and logarithmic enhancement at the low end of β).

The next figure (Fig. 5) shows the $x_{\mathbb{P}}$ distribution for fixed β and Q^2 (values as indicated in each graph). The first row of plots starts at low β with rather flat distributions in $x_{\mathbb{P}}$ (the slope is 0.17 due to soft contributions, $\alpha_{\mathbb{P}}=1.085$). The distributions become slightly more curved and steeper when we move to larger β. The change of the shape with β results

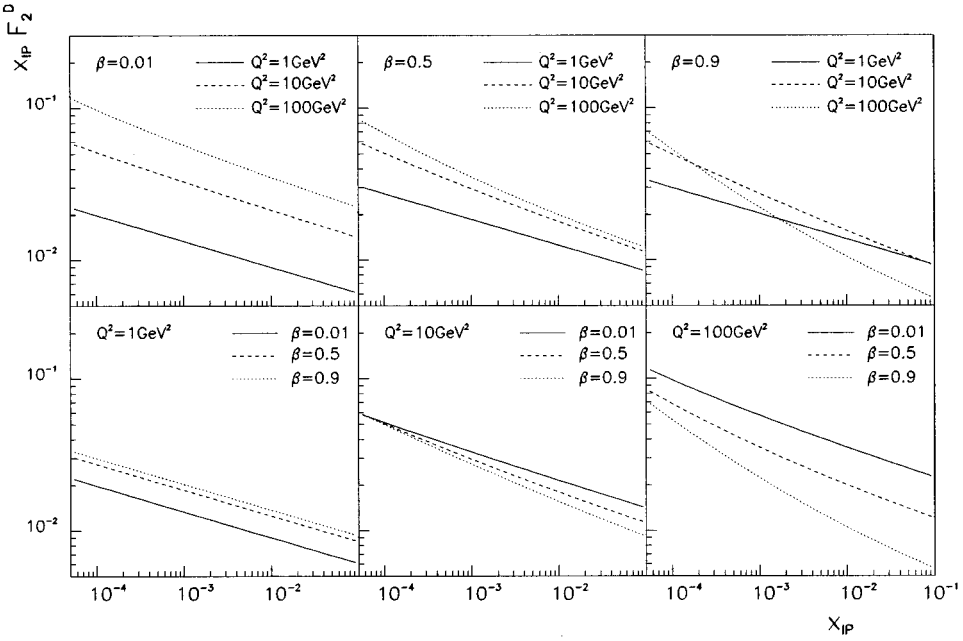

FIG. 5. x_{P} distribution.

from the nonfactorizing ansatz where the Pomeron intercept depends on an intermediated (variable) scale related to the size of the dipole [Q_0^2/v in Eqs. (28), (29), and (30)]. At low β this scale is small (large dipole) and the Pomeron is dominantly soft. At high β and in particular when the higher twist (longitudinal) part takes over the intermediate scale is, in average, rather hard (approximately $Q^2/4$) which leads to steeper distributions. This effect can roughly be interpreted as large mass states having a larger radius than small mass states. The curvature in the double log plots is due to smearing when the scale is integrated. In the second row we see a similar behavior by changing Q^2. At small Q^2 the intercept is frozen at a low (soft) value close to 1.085. There is only a little, barely visible effect due to smearing. When Q^2 is increased the intermediate scale is pulled up and one finds again a steeper and slightly curved distribution. In total we note that Regge-type factorization is violated, i.e., the Pomeron intercept depends on β and Q^2.

The scaling properties in diffraction are of special interest because they provide direct information about the Pomeron structure. Figure 6 shows the dependence of F_2^D on Q^2 for three different values of β (0.01, 0.5, and 0.9) which as we know from Fig. 4 also distinguish between the three contributions F_c, F_a, and F_b. [For very low Q^2 (close to 1 GeV^2) our formula for F_c has to be taken with care, since it is only computed to leading $\ln(Q^2)$ accuracy.] The value for x_{P} is again fixed at 5.0×10^{-4}.

The prediction for the slope in Q^2 is according to usual Q^2 evolution negative at large β. Figure 6, however, shows a rise at low Q^2 for any value of β, even for the longitudinal contribution ($\beta=0.9$). The latter develops a maximum around $Q^2=10$ GeV^2 before the asymptotic regime is reached and the $1/Q^2$ (higher twist) suppression sets in. For $\beta=0.5$ we also see an increase with Q^2 which then flattens out towards a constant (leading twist scaling) behavior. A rise over a certain range in the Q^2 distribution is not completely surprising, since F_2^D vanishes when Q^2 approaches zero. What is surprising is the delay with which the asymptotic (scaling) regime sets in. This effect seems to be model dependent. Taking the hard Pomeron approach from Ref. [29] as example (plots can be found in Ref. [30]) the delay is even more pronounced. A precise measurement of the Q^2-scaling behavior seems to be a promising tool to discriminate various Pomeron models.

A Q^2-scaling violation for rather large β which persists far into the asymptotic region can presumably not be reconciled with the dipole approach. An alternative scenario based on the hard component of the soft Pomeron would predict a $\ln(Q^2)$-type behavior [31].

We have not presented a comparison with data here. This can, however, be found in [32]. The theoretical curve in [32] is based on the same model as presented in this paper, only the values for the parameters have changed slightly with little impact on the x_{P} spectra.

VI. SUMMARY

We have derived the cross section for diffraction in deep inelastic scattering starting from two types of light cone wave functions, one for a quark dipole [Eq. (1)] and the second for a gluon dipole [Eq. (5)]. The latter is of higher

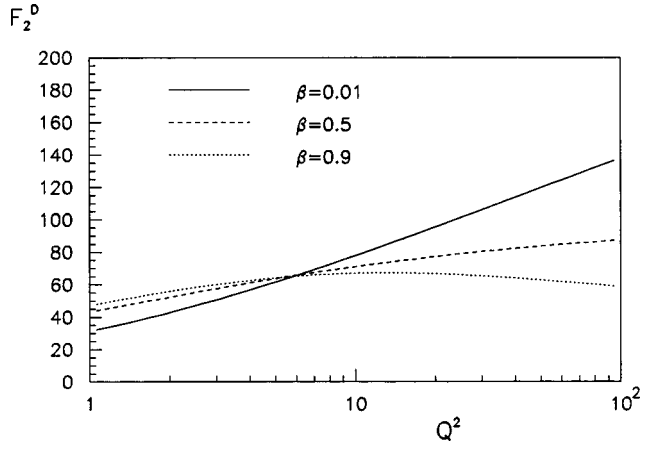

FIG. 6. Q^2 distribution.

order in perturbation theory, since a direct coupling of photons to gluons is lacking. We have shown how the color dipole approach works for a multiparton state provided one stays within the realm of leading twist and leading $\ln(Q^2)$ accuracy (strong ordering in impact parameter space). Only the leading order quark-antiquark pair forms a dipole for any kinematics. The light cone wave function formalism was proven to be consistent with Feynman diagram calculations, but it should not be confused with the general dipole approach of Ref. [33]. As soon as the strong ordering in impact parameter is lost multiple dipoles may occur. The wave function formalism presented here is not able to cope with this configuration.

The expression for the quark dipole (1) is rather well known, the second expression (5) for the two gluon dipole is new. It is valid over the complete range of invariant mass of the two gluons and therefore an extension of an earlier derived version which was limited to large masses [triple Regge limit, Eq. (6)].

As model for the Pomeron we have considered color zero two gluon exchange which is easily generalized to multigluon exchange. All gluons at each leg of the dipole merge into a single vertex, i.e., there is only a single interaction point in impact parameter space. We can factorize the dipole from the target (k_t-factorization scheme) and parametrize all unknown contribution in terms of an unintegrated gluon structure function. This factorization works for two simple perturbative gluons, for shadowing corrections [34], and even for scattering in a nonperturbative classical field. It should be possible to reformulate the results in Ref. [35] along the line of our dipole approach. In the semiclassical approach of Ref. [36] the gluon density is directly related to the unintegrated structure function, and the Landshoff-Nachtmann model [37] can as well be identified with an appropriate unintegrated gluon structure function.

In this paper, however, a more phenomenological ansatz was chosen. A parametrization for the unintegrated structure function was established with parameters determined from inclusive deep inelastic scattering (F_2) and then inserted into the corresponding expression for diffraction. An important feature of our parametrization is the scale dependence of the Pomeron intercept which results in a variation of the x_{P} slope. The scale is roughly the inverse size of the dipole (not Q^2) which has to be integrated over. Its average is close to the soft scale of 1 GeV, but increases slightly with β and Q^2 which then causes the x_{P} distribution to become steeper. The lower limit for the slope is given by the soft Pomeron intercept. The β spectrum is subdivided into three regions each being dominated by the following contributions: (i) the gluon dipole at small β, (ii) the quark dipole with transverse polarized photons at medium β, and (iii) the quark dipole with longitudinal polarized photons (higher twist) at large β. Around $Q^2=10\ \mathrm{GeV}^2$ the total spectrum is rather flat, but it starts tilting when Q^2 is increased (falling from $\beta=0$ to $\beta=1$).

The Q^2 distribution is of special interest because it helps revealing the structure of the Pomeron. We find that for $\beta>0.5$ the slope in Q^2 is positive up to $Q^2\sim 10\ \mathrm{GeV}^2$ and then flattens out (leading twist) or turns down (higher twist at large β) (see Fig. 6). A comparison with data from H1 was performed in Ref. [32] where the agreement is found to be reasonable. The main deviation between theory and data is due to secondary exchanges which have not been included in this paper. The LPS data from ZEUS [28] also seem to agree quite well.

So far only leading order and most important next-to-leading order contributions have been taken into account. To obtain more precise prediction for β and Q^2 distributions one needs to perform a complete Q^2 evolution which will be subject of another publication. Also of interest is a next-to-leading order diffractive jet analysis. This requires, however, a full and consistent next-to-leading order calculation which goes beyond the light cone wave function approach of this paper.

ACKNOWLEDGMENTS

I am very grateful to J. Bartels and A. White for valuable discussions and I thank the Argonne ZEUS group for providing information about data and experiment. This work was supported by the U.S. Department of Energy, Contract No. W-31-109-ENG-38.

[1] ZEUS Collaboration, Z. Phys. C **68**, 569 (1995); **70**, 391 (1996).
[2] H1 Collaboration, Phys. Lett. B **348**, 681 (1995).
[3] A. Donnachie and P. V. Landshoff, Nucl. Phys. **B303**, 634 (1988); **B244**, 322 (1984).
[4] V. S. Fadin, E. A. Kuraev, and L. N. Lipatov, Sov. Phys. JETP **44**, 433 (1976); **45**, 199 (1977); Ya.Ya. Balitskii and L. N. Lipatov, Sov. J. Nucl. Phys. **28**, 822 (1978).
[5] J. Bartels and M. Wüsthoff, Z. Phys. C **66**, 157 (1995).
[6] J. Bartels, Phys. Lett. B **298**, 204 (1993); Z. Phys. C **60**, 471 (1993).
[7] A. Capella, A. Kaidalov, C. Merino, D. Pertermann, and J. Tran Thanh Van, Phys. Rev. D **53**, 2309 (1996); A. Capella, A. Kaidalov, C. Merino, and J. Tran Thanh Van, Phys. Lett. B **337**, 358 (1994).
[8] H. Abramowicz, E. M. Levin, A. Levy, and U. Maor, Phys. Lett. B **269**, 465 (1991).
[9] F. E. Low, Phys. Rev. D **12**, 163 (1975); S. Nussinov, Phys. Rev. Lett. **34**, 1286 (1975).
[10] S. Catani and F. Hautmann, Nucl. Phys. **B427**, 475 (1994).
[11] A. H. Mueller, Nucl. Phys. **B335**, 115 (1990).
[12] N. Nikolaev and B. G. Zakharov, Z. Phys. C **64**, 631 (1994); **53**, 331 (1992).
[13] M. G. Ryskin, Sov. J. Nucl. Phys. **52**, 529 (1990); Nucl. Phys. (Proc. Suppl.) **18C**, 162 (1990).
[14] J. Bartels, H. Lotter, and M. Wüsthoff, Z. Phys. C **68**, 121 (1995).
[15] L. V. Gribov, E. M. Levin, and M. G. Ryskin, Phys. Rep. **100**, 1 (1983).
[16] E. M. Levin and M. G. Ryskin, Report No. LNF-90-025-PT, 1990 (unpublished).

[17] J. Kwiecinski, A. D. Martin, and P. J. Sutton, Phys. Rev. D **46**, 921 (1992).
[18] ZEUS Collaboration, *Measurement of the Total $\gamma^* p$ Cross Section at Very Low x and Q^2 at HERA*, Proceedings of the ICHEP96 Conference, Warsaw, 1996 (unpublished), pp. 02–025.
[19] H1 Collaboration, Nucl. Phys. B **470**, 3 (1996).
[20] E665 Collaboration, Phys. Rev. D **54**, 3006 (1996).
[21] A. D. Martin, M. G. Ryskin, and T. Teubner, Phys. Rev. D **55**, 4329 (1997).
[22] M. Wüsthoff, Report No. DESY-95-166 (unpublished).
[23] M. G. Ryskin and M. Besancon, *Proceedings of the Workshop Physics at HERA*, 1991, edited by W. Buchmüller and G. Ingelman (unpublished), Vol. 1, p. 215.
[24] E. Levin and M. Wüsthoff, Phys. Rev. D **50**, 4306 (1994).
[25] M. Wüsthoff, Ph.D. thesis, Hamburg, 1992.
[26] N. N. Nikolaev and B. G. Zakharov, Phys. Lett. B **332**, 177 (1994).
[27] J. Bartels, H. Lotter, and M. Wüsthoff, Phys. Lett. B **379**, 239 (1996); **B382**, 449(E) (1996).
[28] ZEUS Collaboration, *Measurement of the Cross Section and t Distribution in Diffractive DIS Events with Leading Protons at HERA*, Proceedings of the ICHEP96 Conference, Warsaw, 1996 (unpublished), pp. 02–026.
[29] A. Bialas and R. Peschanski, Phys. Lett. B **387**, 405 (1996); **B378**, 302 (1996).
[30] M. F. McDermott and G. Briskin, in *Hamburg 1995/96, Future physics at HERA*, Proceedings of the Workshop on Future Physics at HERA, Hamburg, Germany, 1995 (unpublished), p. 691.
[31] A. White (private communication).
[32] H1 Collaboration, *A Measurement and QCD Analysis of the Diffractive Structure Function $F_2^{D(3)}$*, Proceedings of the ICHEP96 Conference, Warsaw, 1996 (unpublished), pp. 02–061.
[33] Z. Chen and A. H. Mueller, Nucl. Phys. **B451**, 579 (1995).
[34] E. Gotsman, E. Levin, and U. Maor, Nucl. Phys. **B493**, 354 (1997).
[35] W. Buchmüller, M. F. McDermott, and A. Hebecker, Nucl. Phys. **B487**, 283 (1997).
[36] J. Jalilian-Marian, A. Kovner, A. Leonidov, and H. Weigert, Report No. TPI-MINN-96-28-T, 1997 (unpublished).
[37] M. Diehl, Report No. CPTH-S492-0197, 1997 (unpublished), and references therein.